

Article

Using Particle Swarm Optimization with Backpropagation Neural Networks and Analytic Hierarchy Process to Optimize the Power Generation Performance of Enhanced Geothermal System (EGS)

Ling Zhou ^{1,2}, Peng Yan ^{1,2}, Yanjun Zhang ³, Honglei Lei ⁴, Shuren Hao ^{5,*}, Yueqiang Ma ^{6,*} and Shaoyou Sun ⁷

¹ School of Civil Engineering, Shandong Jianzhu University, Jinan 250101, China; zhouling20@sdjzu.edu.cn (L.Z.); yanpengyix@163.com (P.Y.)

² Key Laboratory of Building Structural Retrofitting and Underground Space Engineering, Shandong Jianzhu University, Jinan 250101, China

³ College of Construction Engineering, Jilin University, Changchun 130026, China; zhangyanj@jlu.edu.cn

⁴ Engineering Research Institute of Appraisal and Strengthening of Shandong Jianzhu University Co., Ltd., Jinan 250014, China; 18204315553@163.com

⁵ School of Civil & Architecture Engineering, East China University of Technology, Nanchang 330013, China

⁶ School of Resources and Safety Engineering, Chongqing University, Chongqing 400044, China

⁷ Beijing General Municipal Engineering Design & Research Institute Co., Ltd., Beijing 100089, China; sunshaoyouwu@sina.com

* Correspondence: haoshuren@ecut.edu.cn (S.H.); mayq@cqu.edu.cn (Y.M.)

Abstract: The optimization of the production scheme for enhanced geothermal systems (EGS) in geothermal fields is crucial for enhancing heat production efficiency and prolonging the lifespan of thermal reservoirs. In this study, the 4100–4300 m granite diorite stratum in the Zhacang geothermal field was taken as the target stratum to establish a numerical model of water-heat coupling of three vertical wells. However, relying solely on numerical simulation for optimization is time-consuming and challenging for the determination of the globally optimal production plan. The present study proposes a comprehensive evaluation method for optimizing the performance of EGS power generation based on the integration of particle swarm optimization with backpropagation neural network (PSO-BPNN) and analytic hierarchy process (AHP). Five different PSO-BPNN models were constructed based on the numerical simulation data to predict different EGS power generation performance indexes, including the production temperature, the injection pressure, the total electricity generation, the electric energy efficiency and the levelized cost of electricity. Based on these PSO-BPNN models, the weights of various thermal development evaluation indexes were calculated by AHP to conduct a comprehensive evaluation of the power generation performance of the three vertical wells EGS. The results show that the PSO-BPNN model has good prediction accuracy for EGS prediction of various performance indicators, with a coefficient of determination (R^2) exceeding 0.999. The AHP evaluation of all production schemes reveals that the optimal power generation scheme entails a well spacing of 580 m, water injection rate of 56 kg/s, injection temperature of 38 °C and fracture permeability of 2.0×10^{-10} m². Over a span of 30 years, this scheme can provide a total power generation capacity amounting to 1775 GWh, with an associated LCOE value of 0.03837 USD/kWh. This not only provides a reference for the development and optimization of geothermal systems in the Zhacang geothermal field but also provides a new idea for the optimization design of other geothermal projects.

Keywords: enhanced geothermal system; optimization; PSO-BPNN models; analytic hierarchy process; LCOE



Citation: Zhou, L.; Yan, P.; Zhang, Y.; Lei, H.; Hao, S.; Ma, Y.; Sun, S. Using Particle Swarm Optimization with Backpropagation Neural Networks and Analytic Hierarchy Process to Optimize the Power Generation Performance of Enhanced Geothermal System (EGS). *Water* **2024**, *16*, 509. <https://doi.org/10.3390/w16030509>

Academic Editor: Giuseppe Oliveto

Received: 29 December 2023

Revised: 29 January 2024

Accepted: 1 February 2024

Published: 5 February 2024



Copyright: © 2024 by the authors. Licensee MDPI, Basel, Switzerland. This article is an open access article distributed under the terms and conditions of the Creative Commons Attribution (CC BY) license (<https://creativecommons.org/licenses/by/4.0/>).

1. Introduction

Background

Geothermal resources are a stable, reliable, green and low-carbon renewable resource, and compared with fossil fuels, geothermal energy is a valuable resource with large reserves and is environmentally friendly and sustainable [1–3]. Since 2010, geothermal energy in China entered into a period of rapid development for the use of heating and cooling buildings and for the generation of electricity [4]. Geothermal energy from Hot Dry Rocks (HDRs) can be used to generate electricity, and an appropriate amount of power stations are established to utilize geothermal energy to generate electricity [5,6]. The annual utilization of geothermal energy is equivalent to saving 25.4 million tons of fuel oil and reducing carbon emissions by 24 million tons per year [7]. Although China has made initial forays into exploring HDR resources and conducting preliminary research on enhanced geothermal system (EGS) technology, it is still in its nascent stages. As of now, China has yet to establish its first EGS demonstration base [8]. The Guide Basin, located in the southeast of Hainan Tibetan Autonomous Prefecture, Qinghai Province, was designated as a geothermal development demonstration area in China [9]. Between 2013 and 2018, two geothermal wells (ZR1 and ZR2) were successfully drilled by the Qinghai Provincial Bureau of Environmental Geological Survey in the Zhacang geothermal field at depths reaching 3050.68 m and 4602 m, respectively. These wells recorded peak temperatures of 151.34 °C and 214 °C, respectively, indicating significant potential for establishing a long-term enhanced geothermal system (EGS) power plant [10]. Consequently, this geothermal field was chosen as the case study.

One of the major challenges facing the industry is to create an economically efficient EGS [11]. A thermal–hydraulic–mechanical multi-field coupling technique underlies the EGS functioning. The operation process of EGS is a multi-field coupling process of the thermal–hydraulic–mechanical (THM) technique [12,13]. Numerical simulation is the most effective and cost-effective method for studying the EGS heat generation process and has been widely used in geothermal fields around the world in recent years [14–17]. Chen et al. [18] considered the influence of open and closed boundary conditions on the temperature drop in the development of HDR reservoirs in the Gonghe Basin. Cui et al. [19] used COMSOL Multiphysics software to establish a vertical two-dimensional planar double pore medium permeability water flow heat transfer model based on the theory of heat-flow-solid coupling. Lous et al. [20] developed a deep-well heat transfer model considering a homogeneous porous medium and investigated the outlet temperature, thermal efficiency and the range of influence of the system, respectively. Wang et al. [21] combined field experiments and numerical simulations to investigate the effects of injection flow rate, injection temperature and flow regime on the heat transfer modeling. Sun et al. [22] established a mathematical model of the THM coupling process in the fractured HDRs and established a fracture–matrix model for the mining process of the EGS project in the Cooper Basin by using the COMSOL Multiphysics numerical simulation software in order to study the heat transfer characteristics in the geothermal reservoirs.

Previous research primarily concentrated on the impact of a single component on an EGS performance index and has not considered the significance of multi-factor interaction on the power generation performance of EGS. The numerical simulation method is accurate in calculation but requires the establishment of many models and consumes a lot of time, so the machine learning method can be introduced to replace numerical simulation to complete a large number of numerical calculations [9,23]. The most commonly used machine learning method in the geothermal field is an artificial neural network (ANN), which is mainly used in EGS drilling position judgment, microseismic prediction and power plant performance optimization [24–26]. Akin et al. [27] proposed the use of ANNs to optimize well location, injection depth and rate for enhanced oil recovery. The predictions were validated using actual drilling data with satisfactory results. Yilmaz et al. [28] analyzed the performance of geothermal power plants through a simulation of geothermal energy production and optimization using the thermal economic cost method combined with ANN.

Optimizing geothermal systems based on economic and safety considerations is a crucial task for sustainable EGS construction. To achieve optimal EGS production, decision-making methods are necessary due to the complex relationship between various influencing factors and geothermal productivity performance indexes, making it challenging to determine the global optimal plan. Currently, the evaluation of geothermal mining primarily relies on a single index, neglecting the comprehensive consideration and quantitative analysis of multiple performance indexes. Consequently, the evaluation results fail to comprehensively account for various factors and lack accuracy in optimizing outcomes [16,17,29,30]. The analytic hierarchy process (AHP) is a widely used decision-making method that has been applied mainly in geothermal energy suitability analysis and geothermal resource potential evaluation [31–33]. In this study, we propose combining neural network techniques with AHP to optimize the EGS production plan, aiming to enhance power generation performance.

In this study, the particle swarm optimization with backpropagation neural network (PSO-BPNN) and AHP methods was introduced to establish a comprehensive evaluation method for the EGS power generation performance of three vertical wells in the Zhacang geothermal field. Firstly, based on the site data of previous studies and indoor experiments, a numerical model of water-heat coupling in three vertical wells was established by using TOUGH2-EOS1 software, and sensitivity analysis was performed to obtain the main influencing factors. Then, a PSO-BPNN model was established by using the numerical simulation data to predict the production temperature (T_{pro}), the injection pressure (P_{inj}), the total electricity generation (W_t), the electric energy efficiency (η_e) and the levelized cost of electricity (LCOE) of the production schemes. Finally, a comprehensive evaluation system was established by using AHP to search for optimal production scenarios of the EGS. This comprehensive evaluation method provides a valuable reference for the EGS optimization of Zhacang geothermal and can be effectively applied to other geothermal development models.

2. Background of the Study Site

The Guide Basin is a Meso-Cenozoic faulted basin in the western part of the West Qinling region of Qinghai Province, China. It is designated as a demonstration area for geothermal development in China. The Zhacang geothermal field is located in the western edge of Guide Basin and developed composite high-temperature geothermal resources (Figure 1). The sedimentary strata in the area are mainly the Neoproterozoic Pliocene Guide Formation (N_2Gd), followed by the Middle–Lower Triassic Longwuhe Formation (T_{1-2l}) and the Quaternary (Q), which are good insulating cover layers. The magmatic rocks in the area are dominated by Late Triassic granodiorite ($T_3\gamma\delta$), mostly distributed in the central and western regions, and the granodiorite fissures and tectonic fracture zones are the tectonic water-bearing thermal storage system [34]. The Zhacang area is controlled by the Hercynian tectonic system, and the main fractures are the Reguang fault (F1) and the Zhacang fault (F5) [35]. The F1 fault is a compressive–torsion reverse fault that blocks water, and the F5 fault is a tension–torsion normal fault that conducts water [36]. The atmospheric precipitation infiltrated through the near east–west tensile fracture zone and was heated by the deep heat source, flowed through the F5 fault and was blocked by the mudstone of the lower disk of the F1 fault and then exposed to the surface to form the Zhacanggou Hot Springs. The hot springs are located at the intersection of two sets of faults, which overflow linearly in the northwest direction. The length of the overflow zone is about 150 m, and there are nearly 30 hot springs exposed, with the flow rate of a single spring ranging from 0.1 to 0.29 L/s, the water temperature ranging from 35 to 93 °C and the total water output ranging from 8.0 to 15.0 L/s [37].

The Qinghai Bureau of Environmental Geology Exploration completed the construction of two geothermal geological drilling wells, ZR1 and ZR2, in the Zhacang geothermal field in 2013. In 2018, logging work was carried out after the construction of the ZR2 well was completed. A total of two fracture-concentrated development zones were

identified, 4210–4220 m and 4310–4320 m, respectively, with fracture orientations in the north-northeast and northeast directions, and the maximum principal stress directions dominated in the northeast and north-northeast directions [10]. Zhang Yu et al. used MIDAS GTS to invert the principal stresses based on the drilling core data of ZR1 and ZR2 wells and the seismic source ground stress survey of the National Electric Power Company, and the results showed that the maximum principal stresses in the thermal reservoirs of 4000–4700 m ranged from 83.2 to 99.1 MPa, and the minimum principal stresses ranged from 61.2 to 75.4 MPa (Figure 2) [29]. The measured temperature of the fissure-type thermal storage at 3000 m in well ZR1 is 151.34 °C, and the measured temperature of the HDR thermal storage at 4600 m in well ZR2 is 214 °C (Figure 2). The average temperature gradient at the basement is about 4.94 °C/100 m, indicating a huge potential for geothermal resources, which means that the Zhacang geothermal field has the potential to build a long-term EGS power plant. Therefore, this field was selected as a case study.

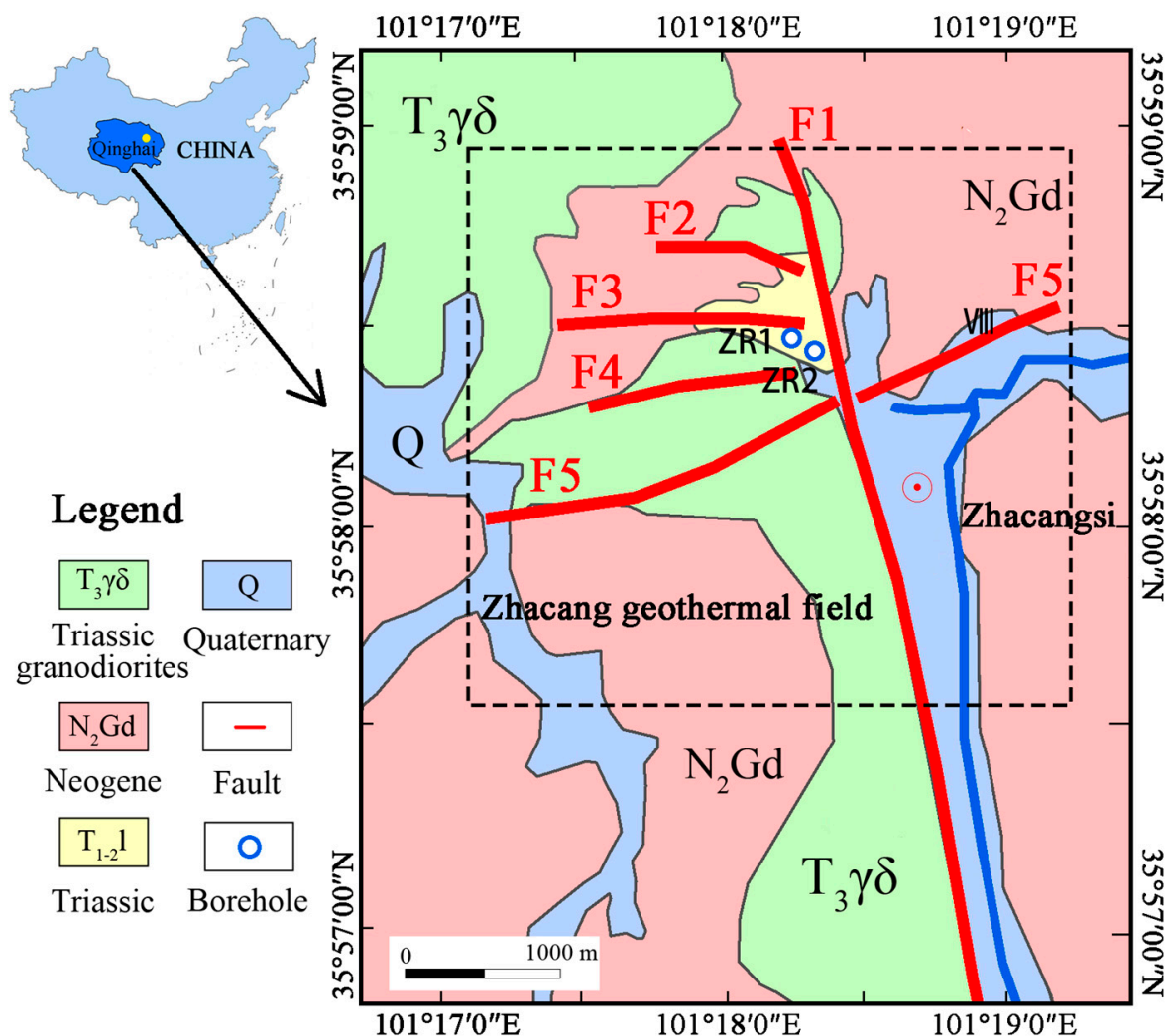


Figure 1. Geological map of the Zhacang area, Guide Basin.

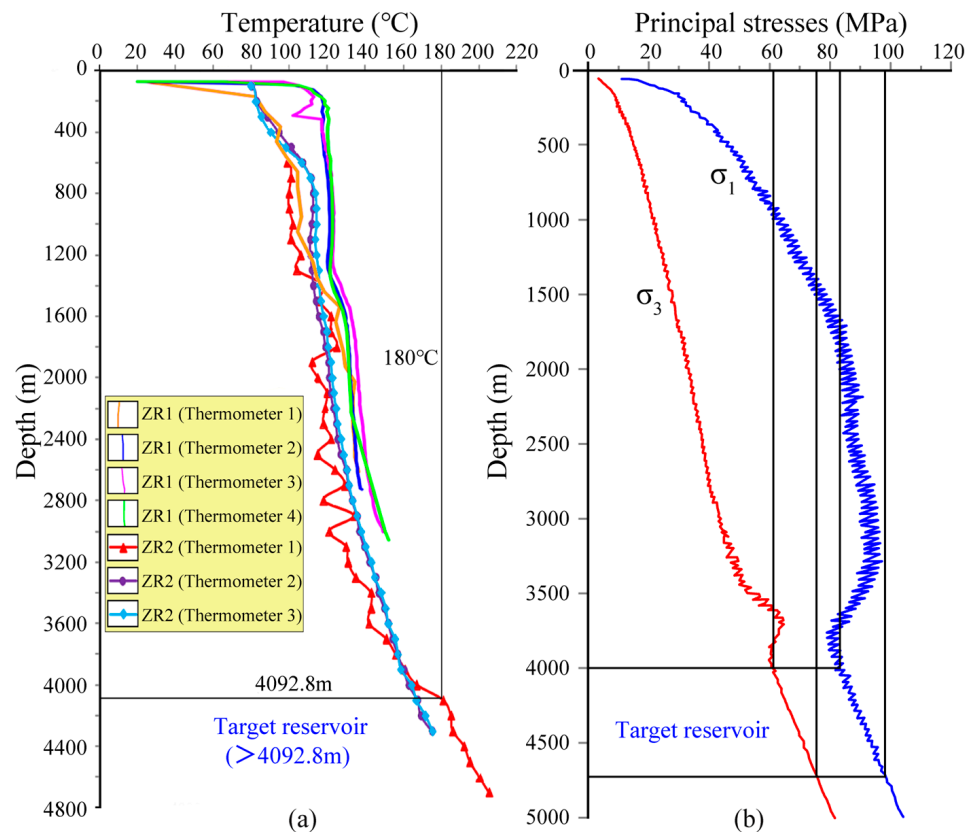


Figure 2. The temperature logs in thermal boreholes (a) and the inversion result of the minimum principal stress (b).

3. Methodology

The present section provides a concise summary of the proposed evaluation method for assessing the performance of EGS power generation based on PSO-BPNN and AHP, aiming to offer valuable insights for vertical-well geothermal extraction in the Zhacang geothermal field.

Firstly, the EGS hydrothermal coupling model of three vertical wells was established using the TOUGH2-EOS1 software. Then, different factors are analyzed, including well spacing, water injection rate and thermal reservoir thermal conductivity. After comparing the degree of influence for each factor, those with significant impacts on EGS power generation performance are selected as optimization objectives: injection temperature, water injection rate, fracture permeability and well spacing. A total of 81 numerical models were established based on different parameters to determine five performance indicators for the system to operate for 30 years, namely, T_{pro} , P_{inj} , W_t , η_e and LCOE.

Secondly, PSO-BPNN was used to estimate the power generation capacity of EGS based on 81 sets of datasets produced by TOUGH2-EOS1 software. Five PSO-BPNN models were built to predict the corresponding five performance indicators, respectively. Prior to training, the data underwent standardization in order to enhance the predictive accuracy of the model. Subsequently, a PSO-BPNN model was employed to forecast power generation performance for 340,000 EGS production schemes.

Lastly, the prediction results obtained from the PSO-BPNN model were utilized to establish an evaluation method for assessing the performance of EGS power generation through the application of analytic hierarchy process. Additionally, considering both production temperature and injection pore pressure restrictions, an optimal production strategy was selected for the Zhacang geothermal field. The flowchart of this study is shown in Figure 3.

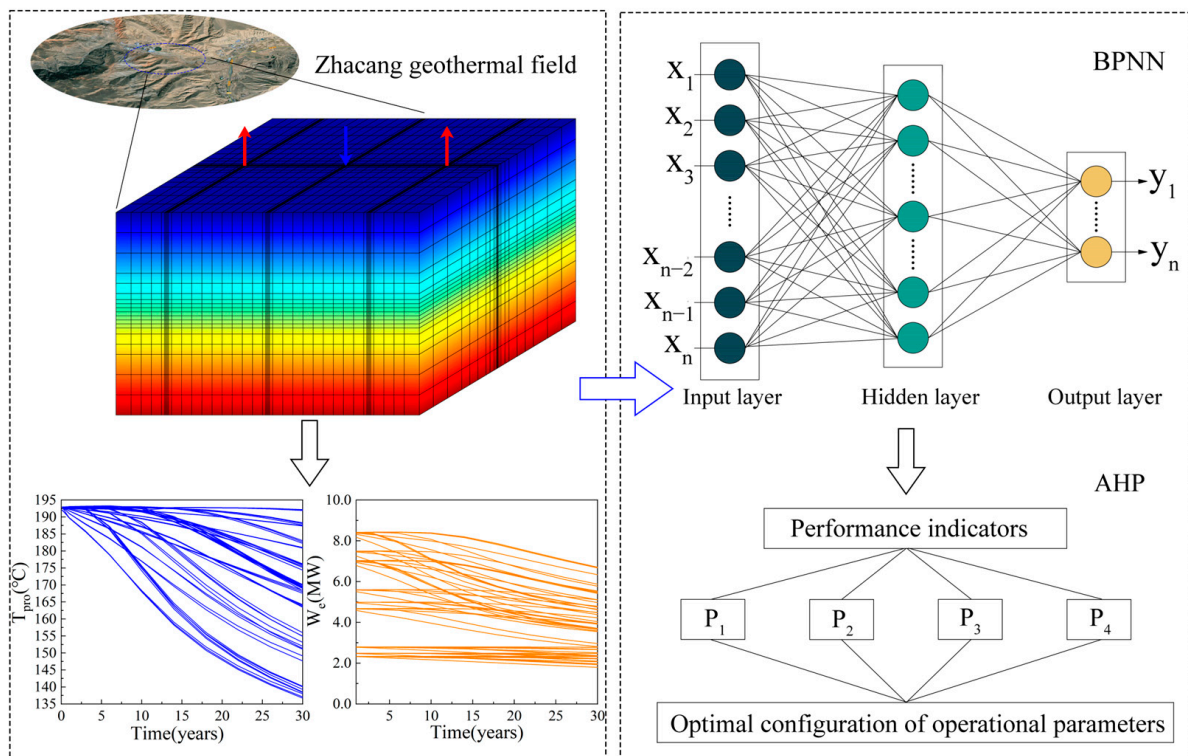


Figure 3. Flowchart in this study.

Lastly, the AHP method is applied to establish an evaluation method for the EGS power generation performance based on the PSO-BPNN strategy prediction results. At the same time, the best production strategy for the Zhacang geothermal field is chosen while taking the constraints of the injection pore pressure and production temperature into account. The flowchart of this study is shown in Figure 3.

4. EGS Numerical Model of Three Vertical Wells

4.1. Modeling and Model Conditions

In this paper, the hydrothermal coupling model of three vertical wells is established using the TOUGH2-EOS1. The EOS1 module of TOUGH2 software is frequently used in the simulation study of geothermal exploitation, and the model is displayed in Figure 4. The hydraulic–thermal coupling model focuses on the strata located at a depth of 3700–4700 m underground within the Zhacang geothermal field. The geothermal system can be divided into three layers, from top to bottom: overburden (400 m), thermal reservoir (200 m) and underlying layer (400 m). It consists of one injection well and two production wells with a designed well spacing of 500 m. Because the original formation is dense granite diorite, hydraulic fracturing is required to increase the porosity and permeability of the thermal reservoir. According to the well logging data, the maximum principal stress direction in the range of 4200–4400 m downhole of ZR2 well is NE-SW direction. The connection direction of three wells should be approximately parallel to the maximum horizontal stress direction, thus ensuring that the injection well and the production well can be connected by hydraulic fracturing. As shown in Figure 4, the model size is 1500 m × 1000 m × 1000 m, with a total of 20,064 units. The artificial fractures extend along the y-direction, and the size is divided according to the extension range of the fracture network after fracturing. In order to improve the accuracy of the simulation results, the grid is refined in the vicinity of the injection well, the production well and reservoirs.

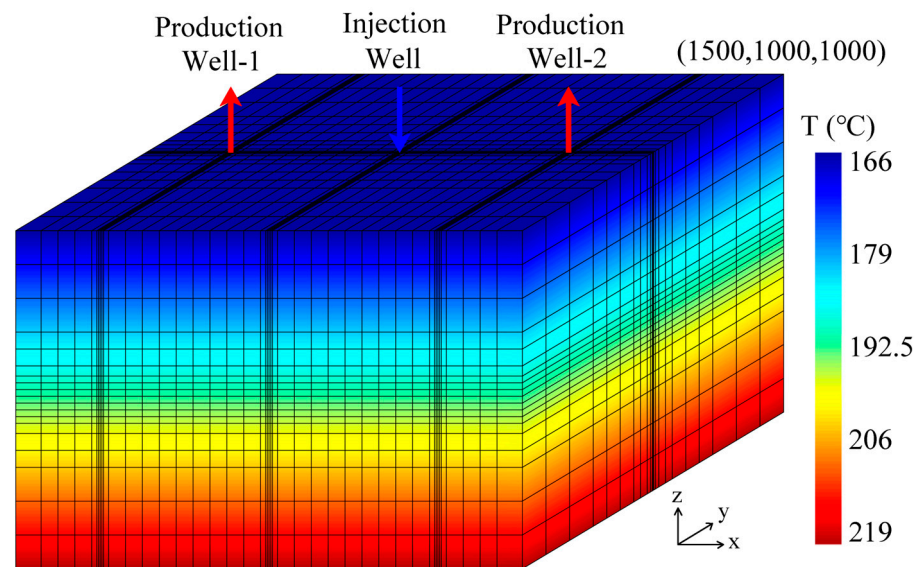


Figure 4. Three-dimensional view of an example reservoir model with the initial temperature distribution.

The initial pore pressure field and temperature field of the numerical model are assigned based on a gradient approach. At the top of the model, the pore water pressure and temperature are set to 37 MPa and 166 °C, respectively, while at the bottom, they are set to 47 MPa and 219 °C. The model boundary is set as no water flow and heat flow exchange. Clear water is used as the heat exchange fluid, and the output fluid is cooled and re-injected into the reservoir after passing through the power station. In the base model, the injection temperature after condensation is set at 50 °C. According to the actual engineering experience of other EGS projects in the world, the injection fluid speed is usually between 5 and 80 kg/s. It is assumed that the water injection speed of a single fracture in the model is 40 kg/s. During the operation of the system, fluid filtration is not considered, and the conductivity of the fracture remains unchanged during the operation. Table 1 presents the relevant parameters of the geothermal mining model. The thermal and physical parameters of reservoir are obtained from laboratory tests, simulating 30 years of EGS operation.

Table 1. Reservoir properties of the base model.

Parameters	Value
Rock density	2711 kg/m ³
Rock porosity	1.86%
Rock permeability ($k_x = k_y = k_z$)	3.66×10^{-16} m ²
Rock thermal conductivity	3.36 W/(m·K)
Rock-specific heat capacity	713 J/(kg·K)
Fracture porosity	50%
Fracture permeability ($k_x = k_y = k_z$)	2.0×10^{-11} m ²
Initial reservoir temperature	$T = 219 - 0.053z$ (°C)
Initial reservoir pressure	$P = 4.7 \times 10^7 - 10,000z$ (Pa)
Productivity index	5.0×10^{-12} m ³
Operation time	30 years

There are many factors that affect the ability of EGS to generate electricity. The internal factors include geothermal gradient (dT/dz), thermal conductivity (λ), fracture permeability (k) and porosity (ϕ_f) after reservoir reconstruction [16,30]. The external factors include water injection temperature (T_{inj}), water injection rate (q) and well spacing (d) [17,29]. This study is based on the base model; the single factor control variable method was used to explore the influence of various factors on each index: (a) reducing

λ to $\lambda = 2.5w/(m \cdot ^\circ\text{C})$, (b) increasing dT/dz to $dT/dz = 6.0 \text{ }^\circ\text{C}/100 \text{ m}$, (c) reducing φ_f to $\varphi_f = 30\%$, (d) increasing k to $k = 2 \times 10^{-10} \text{ m}^2$, (e) reducing T_{inj} to $T_{inj} = 30 \text{ }^\circ\text{C}$, (f) increasing q to $q = 60 \text{ kg/s}$, (g) increasing d to $d = 600 \text{ m}$. Through the analysis of various influencing factors, the factors that have a greater impact on the power generation performance of EGS are selected as the input set of the PSO-BPNN model.

4.2. The Performance Indicators

The power generation performance of EGS is typically comprehensively evaluated using five key performance indicators: T_{pro} , P_{inj} , W_t , η_e , LCOE.

- (1) T_{pro} is the temperature of the production water, $^\circ\text{C}$. In order to ensure the stable power generation of the system, the production temperature drop should be less than 10% during the 15–20 years of designed operating life [38].
- (2) When P_{inj} exceeds the minimum horizontal principal stress of the reservoir, the proppant will relax or even fall off in the reservoir fracture, and the fallen proppant will pile up at the bottom of the fracture, forming a “pipe” with high conductivity, which will result in a thermal short-circuit phenomenon. Therefore, it must be ensured that the injection pressure is not greater than the minimum horizontal principal stress of the reservoir (Equation (1)) [39].

$$P_{inj} \leq \sigma_{hmin} \quad (1)$$

where σ_{hmin} is the minimum horizontal principal stress of the target reservoir, and the minimum principal stress of the reservoir 4100~4300 m below ground is 63.2~67.3 MPa.

- (3) W_t is the total electricity generation by EGS in 30 years (Equations (2)–(4)) [6].

$$W_t = \int_0^{\Gamma_{30}} W_e dt \quad (2)$$

$$W_e = 0.45qf(h_{pro} - h_{inj}) \quad (3)$$

$$f = 1 - T_{rej}/T_{pro} \quad (4)$$

where W_e is the electricity generation rate (MW), the energy conversion efficiency is assumed to be 0.45, h_{pro} is the specific enthalpy of the production fluid (kJ/kg), h_{inj} is the specific enthalpy of the injection fluid (kJ/kg), T_{rej} is the average heat rejection temperature (K), with the annual average temperature of Guide Basin is 7.2 $^\circ\text{C}$, and the heat rejection temperature is 280.35 K.

- (4) The electric energy efficiency (η_e) is defined as the ratio of the total power generation energy to the internal energy consumption, which can be written in Equation (5) [17]. The internal energy consumption (W_p) is the sum of the energy consumption of the injection and production pumps, which can be expressed in Equation (6) [17].

$$W_p = q(P_{inj} - \rho gh_1 + \rho gh_2 - P_{pro})/\rho\eta_p \quad (5)$$

$$\eta_e = \frac{W_e}{W_p} = \frac{0.45\rho\eta_p(h_{pro} - h_{inj})(1 - T_{rej}/T_{pro})}{(P_{inj} - P_{pro}) - \rho g(h_1 - h_2)} \quad (6)$$

where ρ is the density of water (kg/m^3), η_p is the efficiency of the pump, $\eta_p = 80\%$, g is the acceleration of gravity (m/s^2), h_1 is the depth of the injection wells, h_2 is the depth of the production wells, $h_1 = h_2 = 4200 \text{ m}$.

- (5) The levelized cost of electricity (LCOE) is the most commonly used method for evaluating the economics of power plants, which is the present value of costs over the life cycle/present value of electricity generation over the life cycle. This paper uses a simplified LCOE method to evaluate EGS, calculating the total costs of a designed EGS over its life cycle, divided by the total electricity generation over its life cycle. For EGS projects, the total costs can be divided into reservoir exploration cost (C_{exp}),

equipment installation cost (C_{equ}), drilling cost (C_{drill}), reservoir development cost (C_{dev}) and operation and maintenance cost ($C_{O\&M}$). For the Zhacang geothermal field, C_{exp} is about 4.3 M USD [29]. C_{equ} is related to the installed power capacity, and the unit capital cost is estimated to be 2000 USD/kW. Based on the scale of the project, the unit capital cost is estimated at 2000 USD/kW, C_{equ} can be expressed in Equation (7) [40]. C_{drill} is based on the 5100 m GPK3 and GPK4 wells at Soultz EGS in France, which cost 6.57 M USD and 5.14 M USD, respectively [41]. The depth of the three vertical wells in this project is all 4300 m, and C_{drill} can be calculated by Equation (8), where $h_v = 12,900$, $P_v = 1100\%$. C_{dev} can be made up of logging cost and hydraulic fracturing cost. The estimated cost of a high-precision logging at a depth of 4300 m is 4.5 M USD, and the cost of hydraulic fracturing to reservoir modification at a spacing of 300–600 m is 4.5 M USD. $C_{O\&M}$ is usually inversely proportional to the installed capacity and $C_{O\&M}$ can be expressed as Equation (9) [29]. Consequently, C_{total} for the Zhacang EGS power plant can be expressed in Equation (10), and the LCOE can be written in Equation (11).

$$C_{equ} = \frac{2000 \times W_a}{10^3} \quad (7)$$

$$C_{drill} = h_v \times P_v \times 10^{-6} \quad (8)$$

$$C_{O\&M} = \frac{W_t \times 20 \times \exp(-0.0025 \times (W_a - 5))}{10^3} \quad (9)$$

$$C_{total} = C_{exp} + C_{equ} + C_{drill} + C_{dev} + C_{O\&M} \\ = 19.39 + \frac{2000 \times W_a}{10^3} + \frac{W_t \times C_{O\&M}}{10^3} \quad (10)$$

$$LCOE = C_{total} / W_t \quad (11)$$

where W_a is the average electrical power generation (MW).

4.3. Simulation Results and Analysis

Figure 5 shows the evolution of production temperature (T_{pro}), electricity generation rate (W_e), injection pressure (P_{inj}) and electric energy efficiency (η_e) of the base model during a period of 30 years. The T_{pro} decline process can be divided into two stages. In the stable stage (0–10 years), T_{pro} decreased by less than 1%. In the decline stage (10–30 years), the average annual T_{pro} decreased by more than 1%. T_{pro} decreased from the initial 192.5 °C to 169.1 °C (reduced by 12.2%) in the period of 30 years. The trend of W_e was approximately the same as that of T_{pro} ; W_e decreased from 5.0 MW to 3.9 MW (reduced by 21%), which was too large and required further adjustment of the operating parameters to optimize the EGS. During the operation of the system, P_{inj} increased from 54.8 MPa to 62.2 MPa, with an average value of 60.6 MPa. P_{inj} was less than the minimum principal stress (σ_{hmin}) of the reservoir and met the design requirements. η_e during the operation of the system is 3.9. In the early stage of the system operation, the rapid increase of pore pressure at the injection well causes a sharp increase in internal energy consumption, resulting in a sharp drop in η_e .

As depicted in Figure 5a–d, distinct factors exert varying influences on different performance indicators. k , q and d exhibit a greater impact on T_{pro} ; k , T_{inj} and q demonstrate a stronger influence on P_{inj} ; k , T_{inj} , q and d have a more pronounced effect on W_e ; while k , T_{inj} and q possess a higher degree of influence on η_e . Increasing k is more favorable for fluid flow in a thermal reservoir, which can effectively reduce P_{inj} and W_p , so it is beneficial to increase η_e . Meanwhile, increasing k shortens the continuous extraction time of reservoir thermal energy, so the decline speed of T_{pro} and W_e is accelerated. An increase in q will lead to an increase in the extraction of heat from the hot reservoir, and the reservoir temperature will decrease accordingly. T_{pro} will decrease significantly with the increase of q , while W_e will increase significantly. Higher q means more fluid enters the heat exchange channel, resulting in higher P_{inj} and W_p at the bottom of the water injection well, and therefore, η_e will also decrease accordingly. The viscosity of water increases as T_{inj} decreases, leading

to higher P_{inj} . The augmented viscosity hampers fluid circulation within the reservoir, resulting in a rise in W_p and consequently causing a decline in η_e . According to Equation (3), a decrease in T_{inj} will result in an increased enthalpy difference between the injected and produced fluids, leading to a significant increase in W_e . Increasing d means a larger reservoir volume, so more geothermal energy is stored between the injection well and the producing well, so both T_{pro} and W_e increase. At the same time, as d increases, the flow path from the injection well to the producing well will also be extended, resulting in higher P_{inj} .

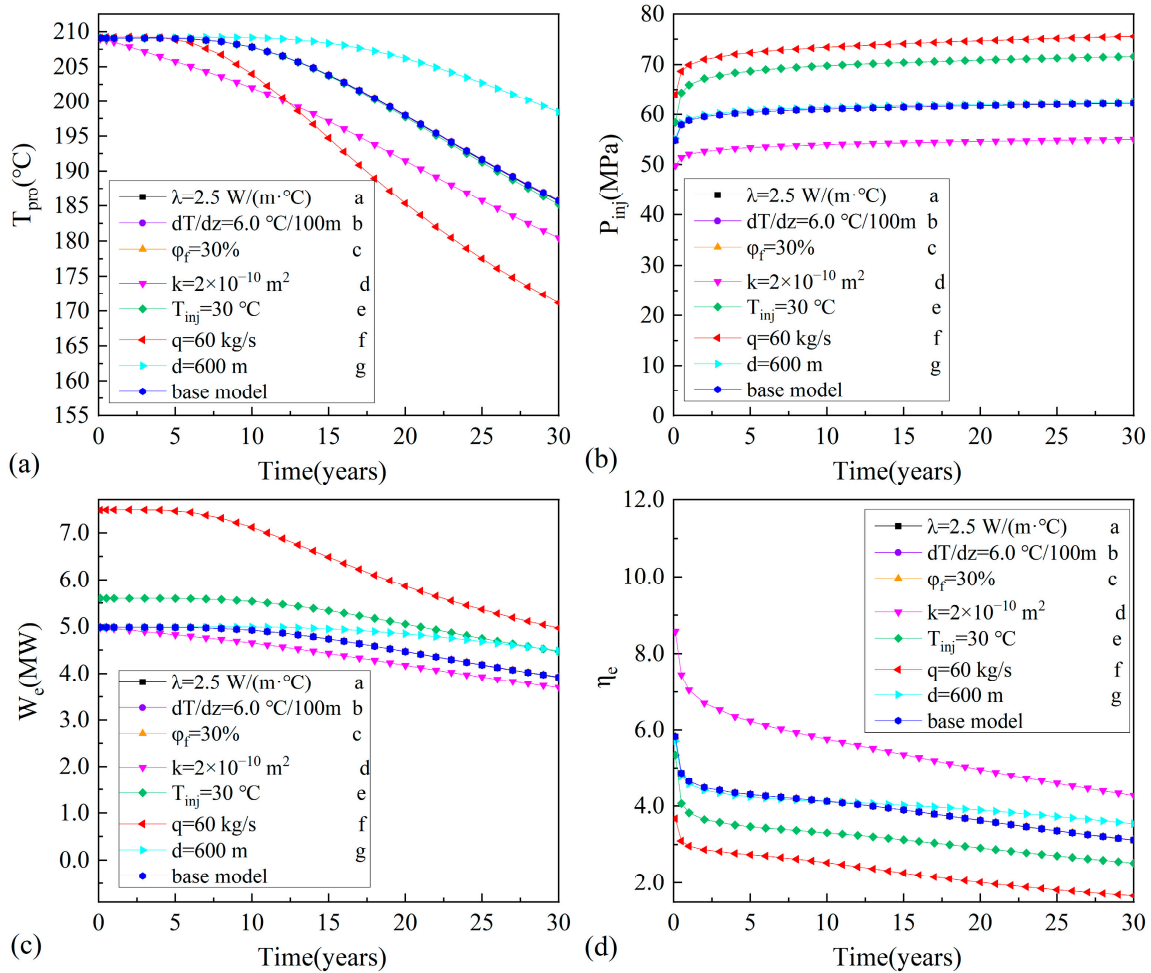


Figure 5. Sensitivity of EGS production indicators to various parameters: (a) production temperature T_{pro} , (b) electricity generation rate W_e , (c) injection pressure P_{inj} and (d) electric energy efficiency η_e .

5. Optimization Model for Power Generation Performance of EGS

5.1. PSO-BPNN Model of EGS

According to the analysis in the above section, well spacing, water injection temperature and velocity and fracture permeability have a great influence on the power generation performance of EGS, and the relationship between each factor and system parameters is not a simple linear relationship. In order to design economical and safe geothermal production schemes and improve the power generation capacity of geothermal power plants, about 340,000 production schemes need to be formed by combining various factors and analyzing the performance indexes of EGS corresponding to each scheme. It can be seen that the workload is too large to be realized. As such, the PSO-BPNN model with numerical simulation is used in this work to estimate EGS power generation performance, providing a foundation for the rational development of geothermal resources in the Zhacang geothermal field.

5.1.1. The Steps of PSO-BPNN

The steps of PSO-BP neural network are as follows (Figure 6):

- (1) Initialization operations are carried out on the parameters of the BP neural network, such as weights and thresholds, to ensure their proper starting values.
- (2) Initialize the parameters of the PSO algorithm, including the velocity and position of the particle, inertia weight and acceleration.
- (3) The fitness of each particle in the population is calculated, and the position and velocity of the particle are continuously updated based on their fitness values to obtain the optimal position for the entire population. Upon meeting the maximum iteration requirement, the algorithm terminates, yielding an optimal solution for network weight and minimum value. This method can be iteratively updated until all requirements are met.
- (4) Until the error satisfies the prediction requirements, the parameters of the network are adjusted in accordance with the estimated error situation between the prediction strategy output value and the actual value.
- (5) The model iterates continuously and, when the allotted number of iterations is reached, outputs the final forecast.

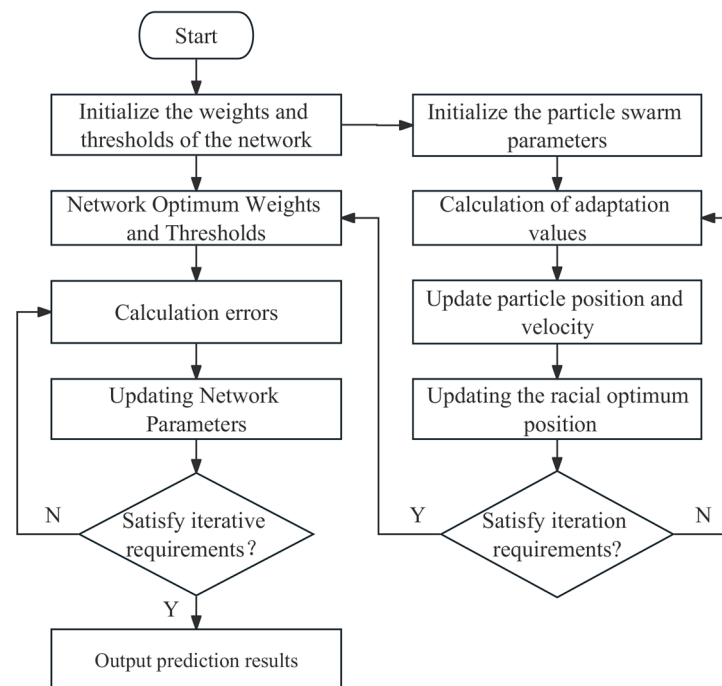


Figure 6. The implementation steps of PSO-BPNN.

5.1.2. Build PSO-BPNN Model

In this study, PSO-BPNN is used to predict the power generation capacity of EGS, and five PSO-BPNN models are constructed to predict T_{pro} , W_t , η_e , P_{inj} and LCOE, respectively. The PSO-BPNN model consists of three components: the input layer, the hidden layer and the output layer. The input layer is comprised of four nodes representing the four factors that influence EGS power generation capacity, including k , T_{inj} , q and d . The output layer includes a node, which is the performance index obtained through numerical simulation, respectively, T_{pro} , P_{inj} , W_t , η_e and LCOE. The number of hidden layer nodes is typically determined using an empirical formula, and in this model, the number of hidden layer nodes is 9. The schematic diagram is shown in Figure 7. The model is set to iterate a maximum of 1000 times, with a training accuracy of 0.0001 and a learning rate of 0.01. The transfer function from the input layer to the hidden layer is tansig, while the transfer function from the hidden layer to the output layer is purelin. The training function employed is trainlm. The data set is from the three vertical well EGS numerical model data

sample in the previous section. The four main influencing factors are set in three cases, respectively (Table 2). A total of $3 \times 3 \times 3 \times 3 = 81$ simulation conditions are set, and each condition is simulated for 30 years. Based on the simulation data, we established a PSO-BPNN prediction model to estimate the generating capacity of an EGS development scheme. To ensure the convergence speed of the PSO-BPNN model is not affected by input data dimensions, we normalized the input data within a range of 0-1. In order to verify the accuracy of the model, 16 groups of data (about 20% of the total data) were randomly selected as the validation set.

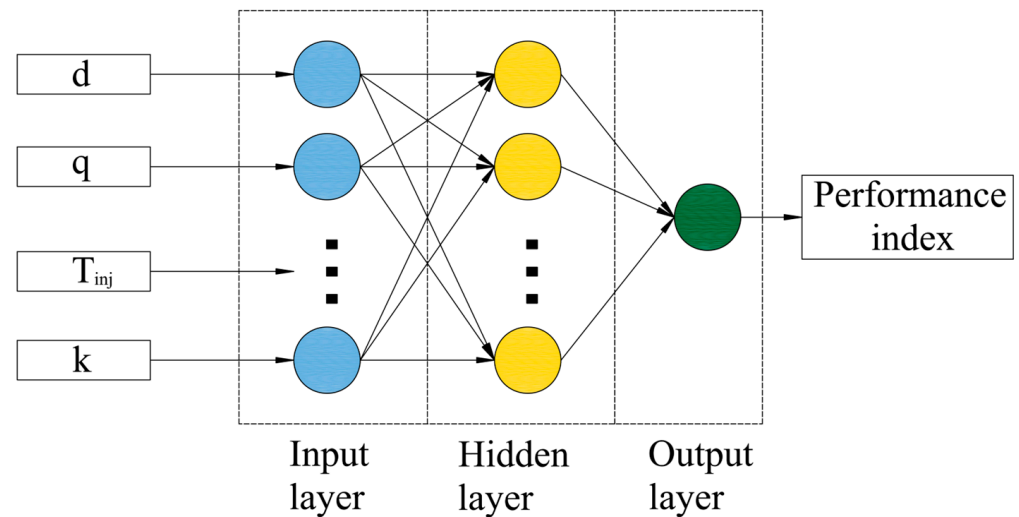


Figure 7. Network architecture of the neural network model for predicting EGS performance index.

Table 2. The values of the four key factors.

	Value		
Well Spacing, d (m)	400	500	600
Water Injection Rate, q (kg/s)	20	40	60
Injection Temperature, T_{inj} ($^{\circ}$ C)	30	50	70
Fracture Permeability, k (m^2)	2×10^{-12}	2×10^{-11}	2×10^{-10}

5.1.3. Prediction Accuracy Evaluation

In order to confirm that PSO-BPNN prediction models are superior, three indices of a mean absolute error MAE , a mean absolute percentage error $MAPE$ and a root mean squared error $RMSE$ are used to evaluate the network performance. MAE , $MAPE$ and $RMSE$ are all positive values, with higher prediction accuracy indicated by lower values, which can be expressed in Equations (12)–(14) [42].

$$MAE = \frac{1}{n} \sum_{i=1}^n |y'_i - y_i| \quad (12)$$

$$MAPE = \frac{100\%}{n} \sum_{i=1}^n \left| \frac{y'_i - y_i}{y_i} \right| \quad (13)$$

$$RMSE = \sqrt{\frac{1}{n} \sum_{i=1}^n (y'_i - y_i)^2} \quad (14)$$

where y_i represents the actual value; y'_i represents the predicted value; \bar{y}_i represents the mean of the actual values; n is the number of samples.

5.2. Evaluation Modeling of EGS Power Generation Performance

In the process of selecting a geothermal production scheme, it is essential to comprehensively consider various influencing factors when evaluating the EGS power generation performance. Therefore, adopting a scientific and effective method becomes necessary. Building upon existing theory related to AHP, this study conducts an evaluation of the power generation performance for three vertical wells in an EGS system. The objective is to provide a geothermal mining strategy that ensures both safety and economic viability for the Zhacang geothermal field. The main steps involved are as follows:

- (1) Establish an evaluation index system, compare each element pairwise and construct a comparative judgment matrix A based on the relative importance of each index (Equation (15)). The construction often employs the 1~9 scale method.

$$A = \begin{bmatrix} a_{11} & a_{12} & \cdots & a_{1n} \\ a_{21} & a_{22} & \cdots & a_{2n} \\ \vdots & \vdots & \vdots & \vdots \\ a_{n1} & a_{n2} & \cdots & a_{nn} \end{bmatrix} \quad (15)$$

- (2) The consistency test is conducted on the constructed comparative judgment matrix. The process of solving the weight of the evaluation index ω_i is essentially the process of solving the eigenvector corresponding to the maximum eigenroot λ_{\max} of the judgment matrix, and the eigenvector represents the importance of each element. The calculation formula is shown in Equations (16) and (17).

$$\omega_i = \frac{W_i}{\sum_{i=1}^n W_i}, \quad i = 1, 2, \dots, n \quad (16)$$

$$W_i = \sqrt[n]{\prod_{j=1}^n a_{ij}}, \quad i = 1, 2, \dots, n \quad (17)$$

where n is the order of the judgment matrix; a_{ij} is the relative importance of the two indicators in the judgment matrix.

- (3) Verify whether the judgment matrix meets the criteria of consistency, $CR \leq 0.1$. When $CR > 0.1$, the matrix needs to be rebuilt if it fails to meet the consistency requirement, which can be expressed in Equations (18) and (19):

$$CR = \frac{CI}{RI} = \frac{(\lambda_{\max} - n)/(n - 1)}{RI} \quad (18)$$

$$\lambda_{\max} = \frac{1}{n} \sum_{i=1}^n \frac{(A\omega)_i}{\omega_i}, \quad i = 1, 2, \dots, n \quad (19)$$

where CI is the consistency index; RI is the random consistency index. When $n = 4$, the $RI = 0.9$ [43].

- (4) Under the condition of satisfying the consistency test, the evaluation of the EGS power generation performance of three vertical wells can be determined according to Equation (20).

$$U = \sum_{i=1}^n E_{Ni} \times \omega_i, \quad i = 1, 2, \dots, n \quad (20)$$

where E_{Ni} is the parameter set of each indicator after standardization.

6. Results and Discussion

6.1. Performance of ANN Models

Figure 8 shows the average T_{pro} , W_t , average η_e and LCOE of the EGS over a period of 30 years with respect to the predicted values of the PSO-BPNN model. The dotted line represents the equivalence between the predicted data obtained from the PSO-BPNN model and the numerical simulation data. The data points are closely clustered around the dotted line, and there is minimal disparity in performance between the training set and the validation set, indicating the robust stability of these models. The solid line is the regression line for all data sets, with the obtained regression line slopes being 0.9990, 0.9980, 1.0007 and 0.9989, respectively. The coefficient of determination (R^2) is generally in the range of 0-1, and the better the performance of the model, the higher the R^2 value. The correlation coefficients of the model are 0.9994, 0.9999, 0.9999 and 0.9999, respectively, all close to 1.0, indicating that the training quality of the PSO-BPNN model is satisfactory, and no serious errors or wrong samples are observed.

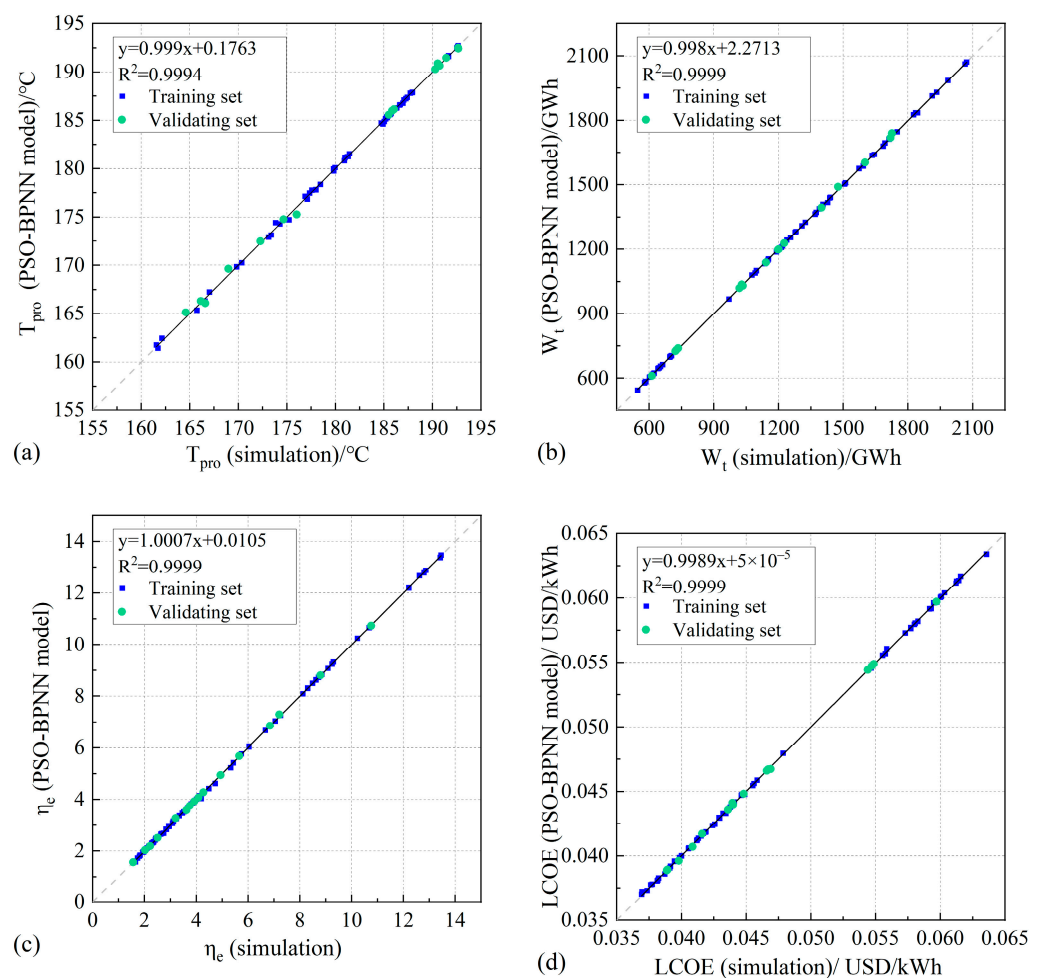


Figure 8. Scatter plots of different targets and their corresponding predictions: (a) average T_{pro} , (b) P_{inj} , (c) average η_e and (d) the LCOE.

The evaluation index reveals that the PSO-BPNN model exhibits superior predictive capability (Table 3). In terms of calculating the average T_{pro} , W_t , average η_e and LCOE of the EGS, the MAE value of the training set in the PSO-BPNN model is lower than that of the BPNN model by 0.0384, 4.8253, 0.0340 and 0.0002, respectively. Additionally, the MAPE value is lower by 0.0205, 0.5347, 0.8535 and 0.5397, respectively, while the RMSE value is lower by 0.0452, 7.3310, 0.0430 and 0.0003. The BPNN model exhibits a reduction in the MAE value of 0.1789, 5.4200, 0.1057 and 0.0002 for the training set, while the MAPE

value shows a decrease of 0.1052, 0.4603, 2.5126 and 0.5788, respectively. Additionally, the RMSE values are reduced by 0.2100, 7.2711, 0.1255 and 0.0004. The prediction accuracy of the PSO-BPNN model surpasses that of the classical BPNN model due to the enhanced global optimization capability achieved by the PSO algorithm through random exploration in particle space. The performance difference between the training set and the validation set is negligibly small, thereby indicating the robust stability of the PSO-BPNN model.

Table 3. Statistical indicator values of BPNN and PSO-BPNN models in different data sets.

Evaluation Indicators	BPNN			PSO-BPNN		
	MAE	MAPE	RMSE	MAE	MAPE	RMSE
Training set						
T_{pro}	0.1589	0.0886	0.2147	0.1205	0.0681	0.1695
W_t	7.1527	0.7486	10.4210	2.3274	0.2139	3.0900
η_e	0.0526	1.3191	0.0721	0.0186	0.4656	0.0291
LCOE	0.0003	0.6650	0.0004	0.0001	0.1253	0.0001
Validating set						
T_{pro}	0.4360	0.2522	0.5521	0.2571	0.1470	0.3421
W_t	9.5780	0.8191	13.2173	4.1580	0.3588	5.9462
η_e	0.1266	3.0370	0.1608	0.0209	0.5244	0.0353
LCOE	0.0003	0.7129	0.0005	0.0001	0.1341	0.0001

6.2. Results of AHP Optimization

In this study, AHP was used to establish a comprehensive evaluation system for the power generation performance of EGS in three vertical wells, as shown in Table 4. The judgment matrix, $CI = 0.0035 < 0.1$, meets the requirements. The weight coefficients of each parameter are calculated to be 0.0827, 0.2668, 0.1540, 0.4965. Therefore, the weight order of each performance index of EGS is $LCOE > W_t > \eta_e > T_{pro}$. The AHP evaluation system of power generation performance is shown in Equation (21). By using this evaluation system, more than 300,000 schemes were evaluated, and the best production scheme was determined. d was 580 m, q was 56 kg/s, T_{inj} was 38 °C, k was 2.0×10^{-10} and the comprehensive score was 0.691, which was higher than the basic (0.551).

$$U = T_{pro} \times 0.0827 + W_t \times 0.2668 + \eta_e \times 0.1540 + LCOE \times 0.4965 \tag{21}$$

Table 4. The weight vector calculation and consistency test of AHP judgment matrix.

A	T_{pro}	W_t	η_e	LCOE	ω	Indicators
T_{pro}	1	1/3	1/2	1/6	0.0827	$\lambda_{max} = 4.010$
W_t	3	1	2	1/2	0.2668	$CI = 0.0035$
η_e	2	1/2	1	1/3	0.1540	$RI = 0.9$
LCOE	6	2	3	1	0.4965	$CR = 0.0038$

6.3. Discussion

Since there are more than 340,000 production schemes, one of every 100 geothermal production schemes is randomly selected and plotted in the figure. Figure 9 shows the LCOE, and the corresponding W_t of the optimal scheme and the random scheme. The random scheme is represented by the blue hollow point, and the optimal scheme is represented by the red solid point. The LCOE decreases with the total power generation, and the decline curve is similar to a hyperbolic curve. The W_t of the optimal scheme is 1775 GWh, and the LCOE is 0.03837 USD/kWh, which is much lower than the industrial electricity cost of Qinghai Province (0.074 USD/kWh). The injection pressure of the random scheme with LCOE less than the optimal scheme is greater than the minimum horizontal principal stress of the reservoir, which does not meet the requirements of safe production.

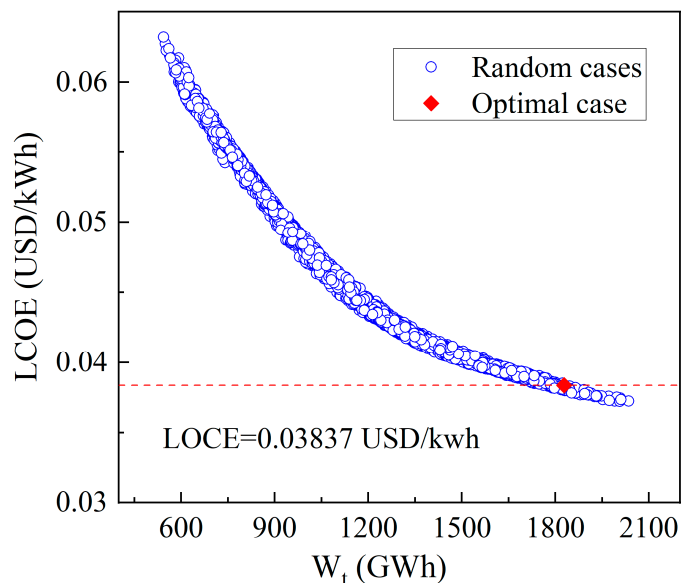


Figure 9. The LCOE and total power generation W_t of random schemes and the optimal scheme.

Figure 10 displays cloud plots depicting the variation of the LCOE under the influence of combined factors. The data in the figure comes from the PSO-BPNN model. The q has the greatest influence on LCOE, and it is significantly greater than other factors. The difference in LCOE under different q schemes can be as high as 0.02 USD/kWh, and under different T_{inj} schemes, it can be as high as 0.005 USD/kWh. Under different d schemes, it can be as high as 0.003 USD/kWh, and under different k schemes, it can be as high as 0.001 USD/kWh. In summary, q has the greatest impact on LCOE, followed by T_{inj} and d , k which has the smallest impact. Smaller LCOE can be obtained by increasing q and d , reducing T_{inj} and k .

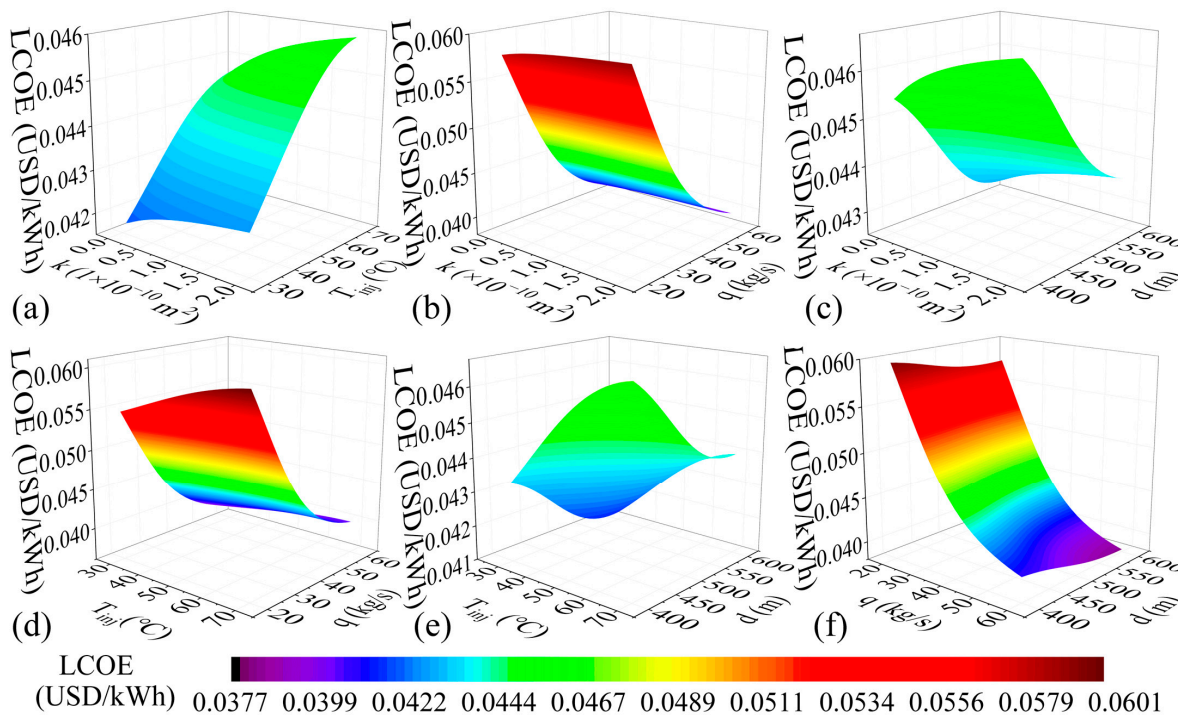


Figure 10. Cloud plot of the LCOE under the influence of combined factors: (a) $k - T_{inj}$, (b) $k - q$, (c) $k - d$, (d) $T_{inj} - q$, (e) $T_{inj} - d$ and (f) $q - d$.

Figure 11 shows T_{pro} of each production scheme in the 30th year. It can be seen that the maximum production temperature is 192 °C and the minimum is 138 °C in all schemes. The T_{pro} of the optimal scheme in the 30th year is 165 °C, which far exceeds the minimum requirements for power generation (105.36 °C) and heating (50 °C). Garnish et al. proposed that T_{pro} drop in an economically successful EGS during the range of 15–20 years should be less than 10% [38]. Therefore, it is assumed that the decrease in T_{pro} within 30 years should be less than 15% (163.63 °C), which is represented by a black dotted line in the figure. The optimal production temperature meets the requirements of economic development and has the potential for long-term power generation.

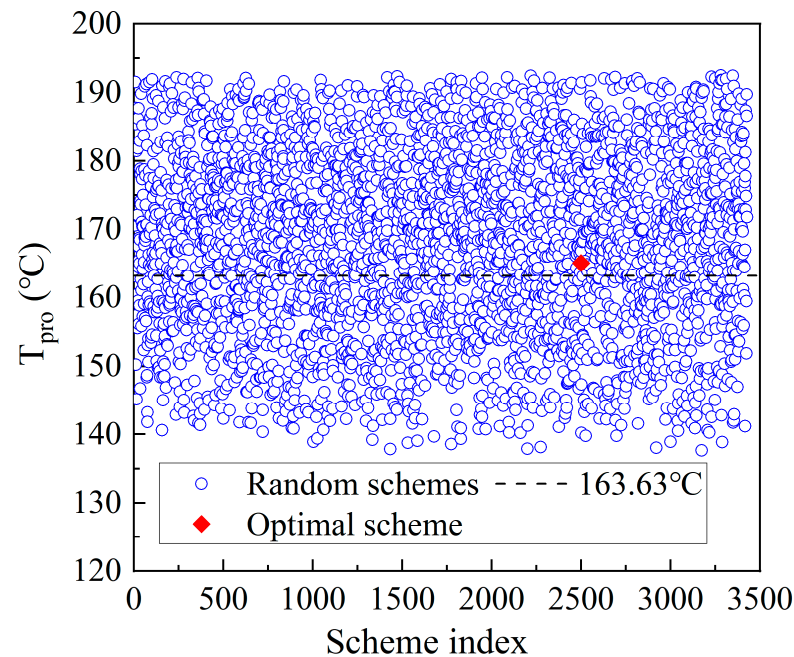


Figure 11. The production temperature T_{pro} in the 30th year of random schemes and the optimal scheme.

Figure 12 shows the average P_{inj} of each production scheme within 30 years. All production schemes exhibit a maximum injection pore pressure of 90 MPa and a minimum of 45 MPa. According to Zhang et al., the minimum horizontal principal stress at the injection bottom is approximately 67.3 MPa [29], as indicated by the black dotted line in the Figure. The P_{inj} of the optimal scheme is 65 MPa, which meets the requirements of safe production. Figure 13 shows the average η_e of each production scheme within 30 years. The average η_e of the optimal scheme is 3.33. The η_e can be enhanced by increasing the value of k and T_{inj} , while reducing q . However, this approach is not favorable for harnessing heat from the thermal reservoir. To achieve higher power generation, it is essential to adopt a scheme with larger q and smaller T_{inj} . Consequently, the average η_e of the optimal production scheme falls to below average.

The findings demonstrate that the utilization of the PSO-BPNN model and AHP for assessing power generation performance can effectively discern the optimal geothermal production schemes in terms of economic feasibility and safety considerations. The time required for modeling to optimization is less than 24 h, whereas the average computational duration of a numerical model amounts to 20 min, and the computation time for 340,000 models totals approximately 9600 h. Consequently, employing the PSO-BPNN model and AHP as a power generation performance evaluation method can significantly enhance optimization efficiency. Moreover, this approach can be directly applied to the other three vertical well EGS projects in order to facilitate further advancement in optimization design. The generalizability of this method can be enhanced from the following perspectives: the ANN algorithm will be optimized to improve the calculation accuracy;

the optimization design schemes of different well numbers and different well types will be designed to achieve the comprehensive optimization of multi-techniques.

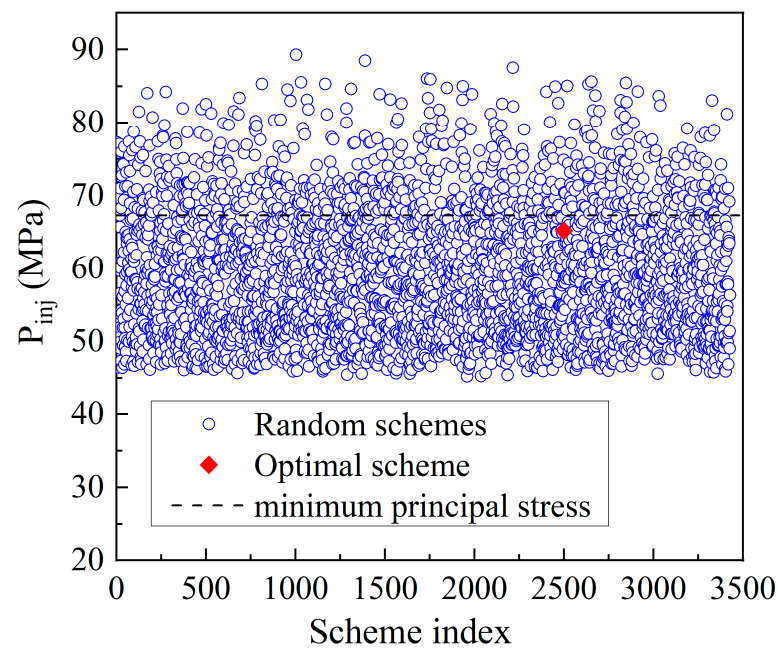


Figure 12. The average injection pressure P_{inj} over a 30-year period in both the random schemes and the optimal scheme.

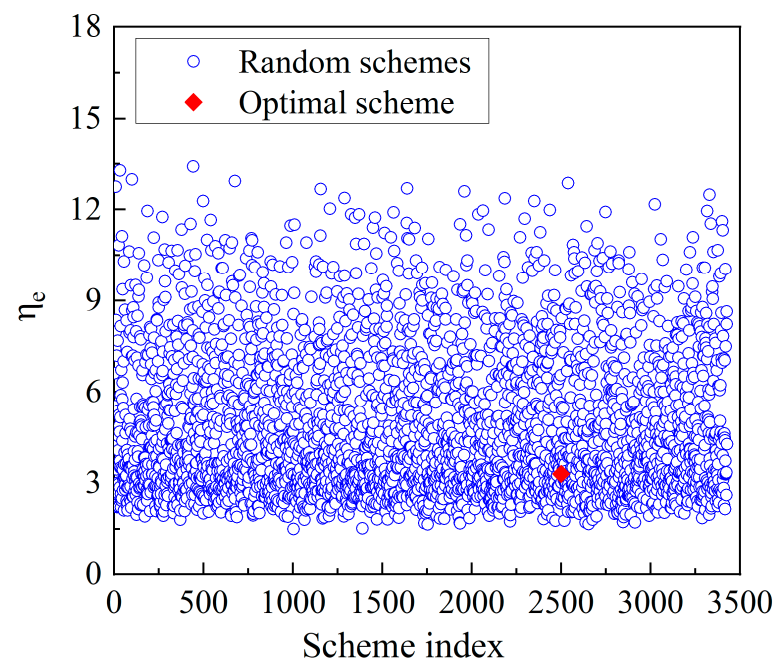


Figure 13. The average electric energy efficiency η_e over a 30-year period in both the random schemes and the optimal scheme.

7. Conclusions

The present study proposes a comprehensive evaluation method for assessing the performance of EGS power generation in the Zhaocang geothermal field, employing PSO-BPNN and AHP techniques to determine the optimal production scheme. The PSO-BPNN model is trained using numerical model data to predict the power generation performance of different production schemes in the Zhaocang geothermal field. Additionally, an AHP

comprehensive evaluation method is established based on various performance indicators to determine the optimal system design for three vertical-well EGSs within a 30-year operation cycle.

The results show that well spacing, water injection rate, injection temperature and fracture permeability are the main influencing factors of EGS in three vertical wells by numerical simulation sensitivity analysis. The PSO-BPNN model has a high accuracy in predicting the accuracy of each performance index within 30 years of EGS with a mean absolute percentage error of about 0.52%, which is 2.51% lower than the BPNN model. In terms of computational speed, the computational time of the PSO-BPNN model is only 1/400 of the numerical model, and the computational efficiency is greatly improved. Based on the AHP comprehensive evaluation method established from the computational data of the PSO-BPNN model, the optimal mining scheme is obtained as well spacing of 580 m, water injection rate of 56 kg/s, injection temperature of 38 °C, fracture permeability of $2.0 \times 10^{-10} \text{ m}^2$, with total power generation of 1775 GWh and LCOE of 0.03837 USD/kWh. It can be seen that this method is effective in EGS optimization and provides considerable profit for the operation of EGS in the Zhacang geothermal field and can also be applied to other similar EGS projects. In future research, more studies need to be conducted to optimize the ANN, improve the computational accuracy and design optimal design schemes for different numbers of wells and different types of wells in order to promote the in-depth development of the optimal design of EGS.

Author Contributions: Conceptualization, L.Z., Y.Z. and H.L.; data curation, L.Z. and H.L.; formal analysis, L.Z., P.Y. and Y.Z.; funding acquisition, L.Z., S.H. and Y.M.; methodology, L.Z. and Y.Z.; project administration, L.Z. and Y.Z.; software, L.Z., Y.Z. and Y.M.; supervision, H.L. and Y.M.; validation, P.Y., S.H., Y.M. and S.S.; visualization, L.Z., Y.Z. and S.H.; writing—original draft, L.Z., P.Y. and S.H.; writing—review and editing, Y.Z., Y.M. and S.S. All authors have read and agreed to the published version of the manuscript.

Funding: The study was funded by the Shandong Natural Science Foundation Youth Fund Project (ZR2021QD123), the National Natural Science Foundation of China (No. 42002258) and the China Postdoctoral Science Foundation (Grant No. 2022M720555).

Data Availability Statement: The data presented in this study are available at <https://github.com/188yan/source-data.git> (accessed on 27 January 2024).

Acknowledgments: We thank the editors and anonymous reviewers for their valuable suggestions for the manuscript.

Conflicts of Interest: Author Honglei Lei was employed by the company Engineering Research Institute of Appraisal and Strengthening of Shandong Jianzhu University Co., Ltd., author Shaoyou Sun was employed by the company Beijing General Municipal Engineering Design & Research Institute Co., Ltd. The remaining authors declare that the research was conducted in the absence of any commercial or financial relationships that could be construed as a potential conflict of interest.

References

1. Kristmannsdóttir, H.; Ármannsson, H. Environmental aspects of geothermal energy utilization. *Geothermics* **2003**, *32*, 451–461. [[CrossRef](#)]
2. Liao, Y.Z.; Liu, Y.G.; Wang, G.L.; Li, T.X.; Liu, F.; Wei, S.C.; Yan, X.X.; Gan, H.N.; Zhang, W. Genesis Mechanisms of Geothermal Resources in Mangkang Geothermal Field, Tibet, China: Evidence from Hydrochemical Characteristics of Geothermal Water. *Water* **2022**, *14*, 4041. [[CrossRef](#)]
3. Zhang, X.; Du, D.; Man, T.; Ge, Z.; Huppert, H. Particle clogging mechanisms in hyporheic exchange with coupled lattice Boltzmann discrete element simulations. *Phys. Fluids* **2024**, *36*, 013312. [[CrossRef](#)]
4. Wang, G.L.; Zhang, W.; Ma, F.; Lin, W.J.; Liang, J.Y.; Zhu, X. Overview on hydrothermal and hot dry rock researches in China. *China Geol.* **2018**, *1*, 273–285. [[CrossRef](#)]
5. Soltani, M.; Farshad, M.K.; Denghani-sanij, A.R.; Kazemi, A.R.; Bordbar, N.; Farshchi, M.J.; Elmi, M.; Gharali, K.; Dusseault, M.B. A comprehensive study of geothermal heating and cooling systems. *Sustain. Cities Soc.* **2019**, *44*, 793–818. [[CrossRef](#)]
6. Lei, Z.H.; Zhang, Y.J.; Yu, Z.W.; Hu, Z.J.; Li, L.Z.; Zhang, S.Q.; Fu, L.; Zhou, L.; Xie, Y.Y. Exploratory research into the enhanced geothermal system power generation project: The Qiabuqia geothermal field, Northwest China. *Renew. Energy* **2019**, *139*, 52–70. [[CrossRef](#)]

7. Lund, J.W.; Freeston, D.H.; Boyd, T.L. Direct application of geothermal energy: 2005 worldwide review. *Geothermics* **2005**, *34*, 691–727. [[CrossRef](#)]
8. Zhang, C.; Hu, S.B.; Huang, R.H.; Wang, Z.T.; Qin, S.; Zuo, Y.H.; Song, Y.C. Research status of heat source mechanism of the hot dry rock geothermal resources and its implications to the studies of genetic mechanism. *Prog. Geophys.* **2022**, *37*, 1907–1919. (In Chinese)
9. Zhou, L.; Zhang, Y.J.; Hu, Z.J.; Yu, Z.W.; Luo, Y.F.; Lei, Y.D.; Lei, H.L.; Lei, Z.H.; Ma, Y.Q. Analysis of influencing factors of the production performance of an enhanced geothermal system (EGS) with numerical simulation and artificial neural network (ANN). *Energy Build.* **2019**, *200*, 31–46. [[CrossRef](#)]
10. Lei, Y.D.; Yuan, Y.J.; Qin, G.X.; Ba, R.S.; Zhao, Z.; Li, T.B. Analysis of Thermal Storage Characteristics of the Guide Zhacang Geothermal Field in Gonghe Basin Based on Logging Data. *Acta Geosci. Sin.* **2023**, *44*, 145–157. (In Chinese)
11. Gudmundsdottir, H.; Horne, R.N. Prediction modeling for geothermal reservoirs using deep learning. In Proceedings of the 45th Workshop on Geothermal Reservoir Engineering, Stanford, CA, USA, 10–12 February 2020.
12. Zhang, X.; Huang, Z.; Lei, Q.; Yao, J.; Gong, L.; Sun, Z.; Li, Y. Impact of fracture shear dilation on long-term heat extraction in Enhanced Geothermal Systems: Insights from a fully-coupled thermo-hydro-mechanical simulation. *Geothermics* **2021**, *96*, 102216. [[CrossRef](#)]
13. Lei, Z.H.; Zhang, Y.L.; Cui, Q.L.; Shi, Y. The injection-production performance of an enhanced geothermal system considering fracture network complexity and thermo-hydro-mechanical coupling in numerical simulations. *Sci. Rep.* **2023**, *13*, 14558. [[CrossRef](#)] [[PubMed](#)]
14. Gong, F.; Guo, T.; Sun, W.; Li, Z.; Yang, B.; Chen, Y.; Qu, Z. Evaluation of geothermal energy extraction in Enhanced Geothermal System (EGS) with multiple fracturing horizontal wells (MFHW). *Renew. Energy* **2020**, *151*, 1339–1351. [[CrossRef](#)]
15. Liao, J.; Xu, B.; Mehmood, F.; Hu, K.; Wang, H.; Hou, Z. Numerical study of the long-term performance of EGS based on discrete fracture network with consideration of fracture deformation. *Renew. Energy* **2023**, *216*, 119045. [[CrossRef](#)]
16. Zhang, C.; Jiang, G.Z.; Jia, X.F.; Li, S.T.; Zhang, S.S.; Hu, D.; Hu, S.B.; Wang, Y.B. Parametric study of the production performance of an enhanced geothermal system: A case study at the Qiabuqia geothermal area, northeast Tibetan plateau. *Renew. Energy* **2018**, *132*, 959–978. [[CrossRef](#)]
17. Xu, T.F.; Yuan, Y.L.; Jia, X.F.; Lei, Y.D.; Li, S.D.; Feng, B.; Hou, Z.Y.; Jiang, Z.J. Prospects of power generation from an enhanced geothermal system by water circulation through two horizontal wells: A case study in the Gonghe Basin, Qinghai Province, China. *Energy* **2018**, *148*, 196–207. [[CrossRef](#)]
18. Chen, T.R.; Liu, G.; Liao, S.M. A comparison study of reservoir boundary conditions of Enhanced Geothermal Systems (EGS). *Energy Procedia* **2019**, *160*, 301–309. [[CrossRef](#)]
19. Cui, H.B.; Tang, J.P.; Jiang, X.T. Influence of permeability on reservoir change during dry hot rock mining. *Hydrogeol. Eng. Geol.* **2020**, *47*, 171–180. (In Chinese)
20. Lous, M.L.; Larroque, F.; Dupuy, A.; Moignard, A. Thermal performance of a deviated deep borehole heat exchanger: Insights from a synthetic coupled heat and flow model. *Geothermics* **2015**, *57*, 157–172. [[CrossRef](#)]
21. Wang, Z.; Wang, F.; Liu, J.; Ma, Z.; Han, E.; Song, M. Field test and numerical investigation on the heat transfer characteristics and optimal design of the heat exchangers of a deep borehole ground source heat pump system. *Energy Convers. Manag.* **2017**, *153*, 603–615. [[CrossRef](#)]
22. Sun, Z.X.; Zhang, X.; Xu, Y.; Yao, J.; Wang, H.X.; Lv, S.; Sun, Z.L.; Huang, Y.; Cai, M.Y.; Huang, X. Numerical simulation of the heat extraction in EGS with thermal-hydraulic-mechanical coupling method based on discrete fractures model. *Energy* **2017**, *120*, 20–33. [[CrossRef](#)]
23. Huang, Z.; Chen, Z.J. Comparison of different machine learning algorithms for predicting the SAGD production performance. *J. Pet. Sci. Eng.* **2021**, *202*, 108559. [[CrossRef](#)]
24. Senturk, A.M. Multi-stage artificial neural network structure-based optimization of geothermal energy powered Kalina cycle. *J. Therm. Anal. Calorim.* **2021**, *145*, 829–849. [[CrossRef](#)]
25. Shahdi, A.; Lee, S.; Karpatne, A.; Nojabaei, B. Exploratory analysis of machine learning methods in predicting subsurface temperature and geothermal gradient of Northeastern United States. *Geotherm. Energy* **2021**, *9*, 18. [[CrossRef](#)]
26. Khosravi, A.; Syri, S. Modeling of geothermal power system equipped with absorption refrigeration and solar energy using multilayer perceptron neural network optimized with imperialist competitive algorithm. *J. Clean. Prod.* **2020**, *276*, 124216. [[CrossRef](#)]
27. Akin, S.; Kok, M.V.; Uraz, I. Optimization of well placement geothermal reservoirs using artificial intelligence. *Comput. Geosci.* **2010**, *36*, 776–785. [[CrossRef](#)]
28. Yilmaz, C.; Koyuncu, I. Thermoeconomic modeling and artificial neural network optimization of Afyon geothermal power plant. *Renew. Energy* **2021**, *163*, 1166–1181. [[CrossRef](#)]
29. Zhang, Y.; Zhang, Y.J.; Zhou, L.; Lei, Z.H.; Guo, L.L.; Zhou, J. Reservoir stimulation design and evaluation of heat exploitation of a two-horizontal-well enhanced geothermal system (EGS) in the Zhacang geothermal field, Northwest China. *Renew. Energy* **2022**, *183*, 330–350. [[CrossRef](#)]
30. Zeng, Y.C.; Tang, L.S.; Wu, N.Y.; Cao, Y.F. Analysis of influencing factors of production performance of enhanced geothermal system: A case study at Yangbajing geothermal field. *Energy* **2017**, *127*, 218–235. [[CrossRef](#)]

31. Dong, J.; He, P.; Liu, H.H.; Guan, Y.; Liu, H.S.; Xia, W.Q.; Dong, J.R. AHP-Based Evaluation of the Suitability of Shallow Geothermal Energy Utilization in GSHP System. *Front. Energy Res.* **2022**, *10*, 3389. [[CrossRef](#)]
32. Yalcin, M.; Sari, F.; Yildiz, A. Exploration of potential geothermal fields using MAXENT and AHP: A case study of the Buyuk Menderes Graben. *Geothermics* **2023**, *114*, 102792. [[CrossRef](#)]
33. Sener, E.; Sener, S. Exploration of geothermal potential using integrated fuzzy logic and analytic hierarchy process (AHP) in Agri, Eastern Turkey. *Turk. J. Earth Sci.* **2021**, *30*, 1134–1150. [[CrossRef](#)]
34. Han, Z.H.; Han, S.J.; Cao, C.G.; Han, Y.S. Petrogenesis and Geological Significance of the Zhacanggou Granodiorite in Guide Basin, Qinghai Province: Constraints from Zircon U Pb Age, Petrogeochemistry and Hf isotope. *J. Jilin Univ.* **2023**, *53*, 177–195. (In Chinese)
35. Jiang, Z.J.; Xu, T.F.; Owen, D.D.R.; Jia, X.F.; Feng, B.; Zhang, Y. Geothermal fluid circulation in the Guide Basin of the northeastern Tibetan Plateau: Isotopic analysis and numerical modeling. *Geothermics* **2018**, *71*, 234–244. [[CrossRef](#)]
36. Lang, X.J.; Lin, W.J.; Liu, Z.M.; Xing, L.X.; Wang, G.L. Hydrochemical characteristics of geothermal water in guide basin. *Earth Sci.* **2016**, *41*, 1723–1734. (In Chinese)
37. Fang, B.; Zhou, X.; Liang, S.H. Characteristics and utilization of the Zhacang hot springs in guide county, Qinghai. *Geoscience* **2009**, *23*, 57–63. (In Chinese)
38. Garnish, J.D. Hot dry rock—a European perspective. *Geotherm. Resour. Coun. Trans.* **1985**, *9*, 329–337.
39. Guo, L.L. *Test and Model Research of Hydraulic Fracturing And Reservoir Damage Evolution in Enhanced Geothermal System*; Jilin University: Changchun, China, 2016.
40. César, R.C.; Mondéjar, R.; Segovia, C.; Martín, A.V. World geothermal power production status: Energy, environmental and economic study of high enthalpy technologies. *Energy* **2012**, *42*, 10–18.
41. Lukawski, M.Z.; Anderson, B.; Augustine, C.; Capuano, L.E.; Beckers, K.F.; Livesay, B. Cost analysis of oil, gas, and geothermal well drilling. *J. Petroleum. Sci. Eng.* **2014**, *118*, 1–14. [[CrossRef](#)]
42. Tibshirani, R.; Walther, G.; Hastie, T. Estimating the number of clusters in a data set via the gap statistic. *J. R. Stat. Soc. Ser. B* **2001**, *63*, 411–423. [[CrossRef](#)]
43. Saaty, T.L. *Multicriteria Decision Making: The Analytic Hierarchy Process*; McGraw-Hill: New York, NY, USA, 1980.

Disclaimer/Publisher’s Note: The statements, opinions and data contained in all publications are solely those of the individual author(s) and contributor(s) and not of MDPI and/or the editor(s). MDPI and/or the editor(s) disclaim responsibility for any injury to people or property resulting from any ideas, methods, instructions or products referred to in the content.